Revista Mexicana de Física **70** 041601 1-9 JULY-AUGUST 2024

DFT formalism studies on the structural and electronic properties of hexagonal graphene quantum dot with B, N and Si substitutional impurities

K. M. Méndez-Martínez[a], F. M. Nava-Maldonado[b,*],
K. A. Rodríguez-Magdaleno[b], C. Ríos-Martínez[a], J. C. Martínez-Orozco[c]

[a] *Unidad Académica de Estudios Nucleares, Universidad Autónoma de Zacatecas, Ciprés 10, Fracc. La Peñuela, 98060, Zacatecas, Zac., Mexico.*
[b] *Unidad Académica de Ciencias Químicas, Universidad Autónoma de Zacatecas, Carretera Zacatecas-Guadalajara Km. 6. Ejido la Escondida, 98160, Zacatecas, Zac., México.*
[*] *e-mail: flavionava@uaz.edu.mx*
[c] *Unidad Académica de Física, Universidad Autónoma de Zacatecas, Calzada Solidaridad esquina con Paseo La Bufa S/N. 98060, Zacatecas, Zac., México.*

Received 9 November 2023; accepted 22 February 2024

The study of carbon-based nanostructured materials is a highly active research field that has made significan progress in the study of two-dimensional materials and nanotechnology. The interest in these materials is mainly attributed to the fascinating properties they exhibit, as seen in the case of graphene as a 2D material, as well as emergence on numerous novel 2D materials and their heterostructures. Additionally, there is important interest in systems such as 2D quantum dots. Therefore, this work focuses on the systematic study of graphene quantum dots of various sizes, all within the framework of first-principle density functional theory. We started with the simplest graphene quantum dot (GQD) structure, benzene (C_6H_6), which consist of six carbon atoms passivated with hydrogen atoms. We then increased its size by adding more aromatic rings, resulting in the following GQD configurations $C_{24}H_{12}$, $C_{54}H_{18}$, $C_{96}H_{24}$, $C_{150}H_{30}$ and $C_{216}H_{36}$. We report the density of states (DOS) and the imaginary part of the dielectric function (ε_2) for the system, analyzing both the pristine configuratio and the effect of both single and double (boron, nitrogen and silicon, denoted as S_a). The double substitutional atom study was done considering random, *ortho*-, *meta*-, and *para*-director positions just for the $C_{94}H_{24}S_{a_2}$ GQD. In general, we can conclude that as the GQD increases in size, the HOMO-LUMO energy decreases. Furthermore, it is observed that boron and nitrogen exhibit their expected n-, and p-type doping characteristics, but this differs between single and double S_a substitutions. Additionally, the imaginary part of the dielectric function is highly sensitive to the positions of single and double substitutional atoms, as well as the polarization of incident light. Therefore, we suggest that these differences can be used to clearly determinate the type of substitutional atoms and their positions from optical measurements.

Keywords: Graphene quantum dots; density functional theory; dielectric function.

DOI: https://doi.org/10.31349/RevMexFis.70.041601

1. Introduction

Carbon exist or is present in nature in two allotropic forms: diamond and graphite. It can also be synthesized as fullerene or as single- and multi-walled carbon nanotubes. Furthermore, in 2004, a new carbon allotrope, graphene, was discovered [1]. Graphene was considered the primary 2D-material since then and is still highly relevant today. Additionally, there are several novel two-dimensional materials, such as the borophene, phosphorene, silicene, germanene, etc., which plays an important role in materials research. These materials have been studied both theoretical and experimentally over the last two decades. The studies on hexagonal two-dimensional materials are not limited to group-IV elements; they have also been extended to III-V ones [2,3], as well as to other 2D-materials like transition metal dichalcogenides [4].

Not only have been extended 2D-materials, ideally infi nite 2D sheets of atoms, studied over the last two decades, but also finit ones that we can categorize as 2D quantum dots have been widely studied for their fascinating properties and potential applications [5,6]. Various synthesis methods can be used to produce carbon nanotubes, fullerenes, or graphene quantum dot structures [7-9]. From a theoretical point of view, there is recent report on the electronic and magnetic properties for double and triple vertically stacked triangular graphene quantum dots with AA and AB atom alignment [10]. There are also reports on the same properties in other materials, such as a single MoS_2 triangular quantum dot [11]. Both of these studies utilize density functional theory (DFT). Furthermore, using DFT, magnetic properties and the tunable band gap of silicene quantum dots embedded in silicane have been reported [12].

One of the most studied graphene quantum dots (GQDs) is the coronene. It is noteworthy for its significance being just after the benzene molecule. Coronene is formed by 24 carbon atoms surrounded by 12 hydrogen atoms (C_mH_n). In this context, m represents the number of carbon atoms in the hexagonal structure, and n represents the number of outer passivating hydrogens. For instance, J.J. Hernández-Rosas *et al.* [13] reported the electrical and chemical properties of the $C_{24}H_{12}$ GQD, they also investigated the graphane and a graphene oxide configuration from the theoretical point

of view, using DFT. In their work, the authors suggested that is possible to control the electronic properties through the adsorbed chemical radicals. The experimental bottom-up preparation has been recently reported [14], along with electronic structure computation, of what the authors called the 24π aromatic coronene molecule. The same $C_{24}H_{12}$ GQD molecule, using DFT, has been studied for the adsorption of neutral and cationic forms of lithium (Li/Li^+) atoms and concluded that the HOMO-LUMO energy level strongly depends on the Li/Li^+ adsorption position [15], and there are some other reports for the same system [16-18].

But there are larger possible configuration for the C_mH_n GQD, as the one reported in Ref. [19] that study the interaction of small molecules with the pristine and N-, Si-, B-, and Al-doped GQD for (m,n) = (24,12), (54,18), and (96,30), with potential applications as gas sensors. The oxygen reduction reaction, as function of the C_mH_n GQD size, has been reported for nitrogen doped systems [20]. The catalytic properties of nitrogen-doped graphene quantum dots (gN-GQDs) in the oxygen reduction reaction (OOR), using different ions/groups absorbed on the GQD surface, have been reported by Q. Guo *et al.* [21]. They concluded that H_3O adsorption exhibits the best ORR catalytic activity compared with the H_3O^+, OH, OH^-, H_3O^+. The theoretical study of the effect of a porphyrin-like vacancy on the spectral properties of graphene quantum dots is reported in Ref. [22], and the authors state that this type of vacancy can modify the charge separation in the excited states of the peripheral carbon chain. Also, the pristine and holey C_mH_n GQD optoelectronic properties has been reported [23], as well as other recent reports [24,25].

The aim of this work is to report the effect of single and double (with random, *ortho*-, *meta*-, and *para*-director positions) boron (B), nitrogen (N), and silicon (Si) substitutional doping atoms on the energetic positions of the Highest Occupied Molecular Orbital (HOMO) and Lowest Unoccupied Molecular Orbital (LUMO), as well as on the density of states (DOS) and the imaginary part of the dielectric function for hexagonally shaped C_mH_n graphene quantum dots (GQDs).

To accomplish this task, in the following sections, we will present the computational methods. Next we will independently present the results for single and double substitutional impurities, with the corresponding discussion. Finally, we will provide the main conclusions of the work.

2. Computational method

In this paper we report the density of states (DOS) as well as the imaginary part for the dielectric function (ε_2) for several hexagonal graphene quantum dots (GQDs). Starting from the simplest possible aromatic structure C_6H_6, a benzene molecule and adding each time more aromatic rings we can reach the $C_{216}H_{36}$ graphene quantum dot structure. We study these systems within the framework of the Density Functional Theory (DFT) by using the SIESTA (Spanish Initiative for Electronic Simulation with Thousand of Atoms) code method implementation [26,27], that uses a linear combination of atomic orbitals (LCAO). Here we implemented a double ζ polarized (DZP) basis set, with a Pseudo Atomic Orbitals (PAO) energy shift of 0.075 eV, for all the reported cases, and the generalized gradient approximation (GGA) exchange and correlation functional with the Perdew-Burke-Ernzerhof (PBE) parametrization. A mesh cutoff energy of 200 Ry, after performing a total energy convergence test for each GQD size, ensures the accuracy of the total energy. Finally, a maximum force tolerance of 0.04 eV/Å has been applied during the relaxation procedure using the conjugate gradients method.

3. Results and discussion

The purpose of this study is to report the DOS and ε_2 for hydrogenated hexagonal GQDs. For this study we start from the well-known benzene molecule (C_6H_6) that consist of six carbon atoms, located at the hexagon vertices that are passivated with hydrogen atoms, as depicted in Fig. 1a). The next hexagonal GQD consist of 24 carbon atoms with 12 passivating hydrogen ones ($C_{24}H_{12}$), as the one in Fig. 1b), that recently has been experimentally synthesized [14], and named coronene. Following this line, we theoretically construct the $C_{54}H_{18}$ GQD depicted in Fig. 1c), then one more aromatic

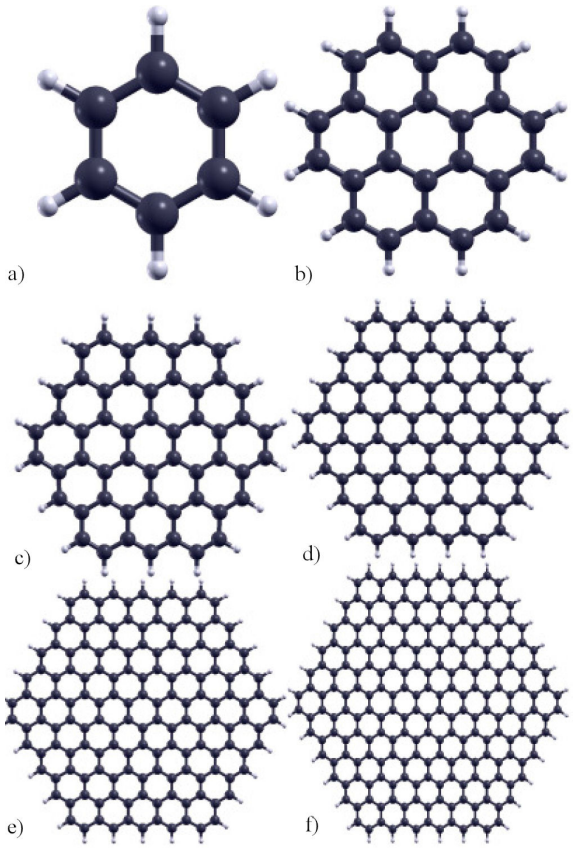

FIGURE 1. Pristine GQD starting from a) benzene (C_6H_6) and increasing the GQD size by adding each time more aromatic rings: b) $C_{24}H_{12}$, c) $C_{54}H_{18}$, d) $C_{96}H_{24}$, e) $C_{150}H_{30}$ and f) $C_{216}H_{36}$.

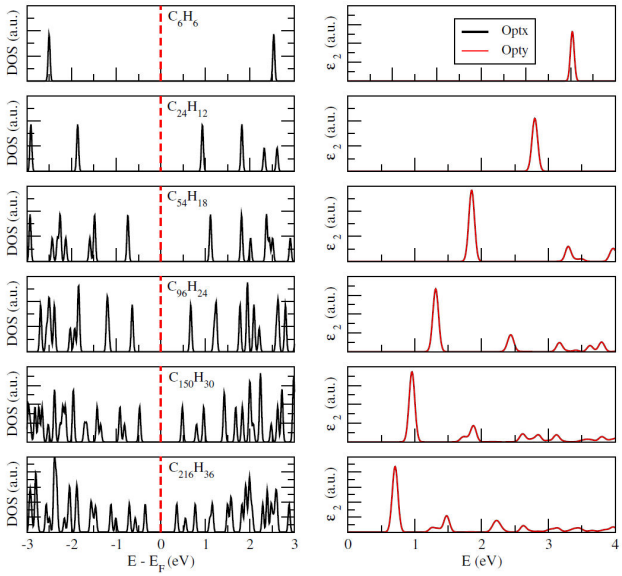

FIGURE 2. Density of states computation, and the imaginary part of the dielectric function, for the hexagonal GQDs depicted in Fig. 1 as the size of the system increases.

ring is added to have in Fig. 1d) the $C_{96}H_{24}$ GQD, followed by the $C_{150}H_{30}$ system in Fig. 1e), and finall the $C_{216}H_{36}$ GQD given in Fig. 1f).

Figure 2 shown, from top to bottom, the DOS as well as the imaginary part of the dielectric function for the C_mH_n hexagonal GQD, for the relaxed structures depicted in Fig. 1, starting from the benzene molecule (C_6H_6), reproducing the characteristic benzene molecule's HOMO-LUMO peaks position. In this case, the HOMO-LUMO energetic distance is about 5.043 eV, that is in good agreement with previous reported theoretical reports [28], the same is true for the $C_{24}H_{12}$ GQD [13]. We can see that as the C_mH_n hexagonal GQDs size increase, by adding each time more aromatic rings, the DOS peak structure is more rich while the HOMO-LUMO energetic distance decreases each time more. In the same fashion, as the C_mH_n hexagonal GQDs size increase, ε_2 exhibits more structure each time, while the optical gap - which must be understood as the energetic distance between zero and the firs imaginary part of the dielectric function peak, also decreases. It is important to mention that we do not apply any optical gap correction to compensate the GGA-PBE underestimated HOMO-LUMO gap or the excitation effects; the same holds for all the ε_2 results reported elsewhere. The *Optx* and *Opty* labels refers to polarized light with electric fiel along x- and y-directions, respectively, and the GQD lies in the x-y plane. All the computed HOMO-LUMO energetic difference, for the C_mH_n GQG systems, are reported in table I. In principle, as the system size increases, the HOMO-LUMO will tend to approach zero, and the density of states (DOS) curve will increasingly resemble the well-known Dirac cone of graphene.

TABLE I. HOMO-LUMO energetic difference for the C_mH_n GQG.

	C_6H_6	$C_{24}H_{12}$	$C_{54}H_{18}$
HOMO-LUMO (eV)	5.043	2.797	1.862
	$C_{96}H_{24}$	$C_{150}H_{30}$	$C_{216}H_{36}$
HOMO-LUMO (eV)	1.321	0.958	0.716

3.1. GQD properties with substitutional impurities

In this section, we analyze the effect of considering substitutional impurities on the structural properties, density of states, as well as the imaginary part of the dielectric function of the system, with x- and y-direction polarized light. We use substitutional impurities from the nearest neighboring carbon atoms, which are boron (B), nitrogen (N), and silicon (Si). First, a single substitutional atom, located at one vertex of the central hexagon for the three largest C_mH_n hexagonal GQD, is considered. Then, we consider the intermediate $C_{96}H_{24}$ hexagonal GQD configuratio with two substitutional impurity atoms, in the central aromatic ring, with *ortho*-, *meta*-, and *para*-director positions, as well as one in the central aromatic ring and the other in a random position.

3.1.1. *GQD with single substitutional impurities*

In Fig. 3a) we present the relaxed structure for an hexagonal $C_{96}H_{24}$ pristine graphene quantum dot with a carbon-carbon interatomic distance of 1.44 Å. In Fig. 3b), the relaxed system, considering a boron substitutional impurity in the central hexagonal carbon ring is presented, with a carbon-boron interatomic distance of 1.50 Å. When a nitrogen atom, depicted un Fig. 3c), is considered instead of the carbon atom, the interatomic carbon-nitrogen distance is 1.42 Å. Finally, when the silicon atom, the larger one, substitutes the same carbon

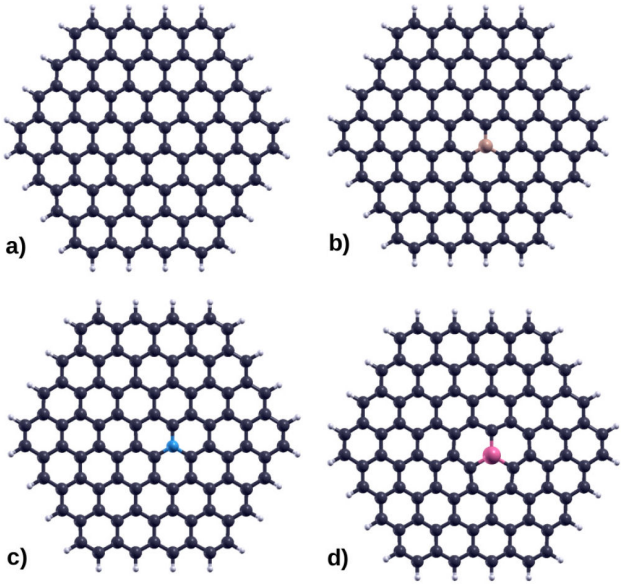

FIGURE 3. Hexagonal $C_{96}H_{24}$ GQD a) without doping, b) considering a B substitutional atom ($C_{95}H_{24}B$), c) a N substitutional atom ($C_{95}H_{24}N$), and d) a Si substitutional atom ($C_{95}H_{24}Si$).

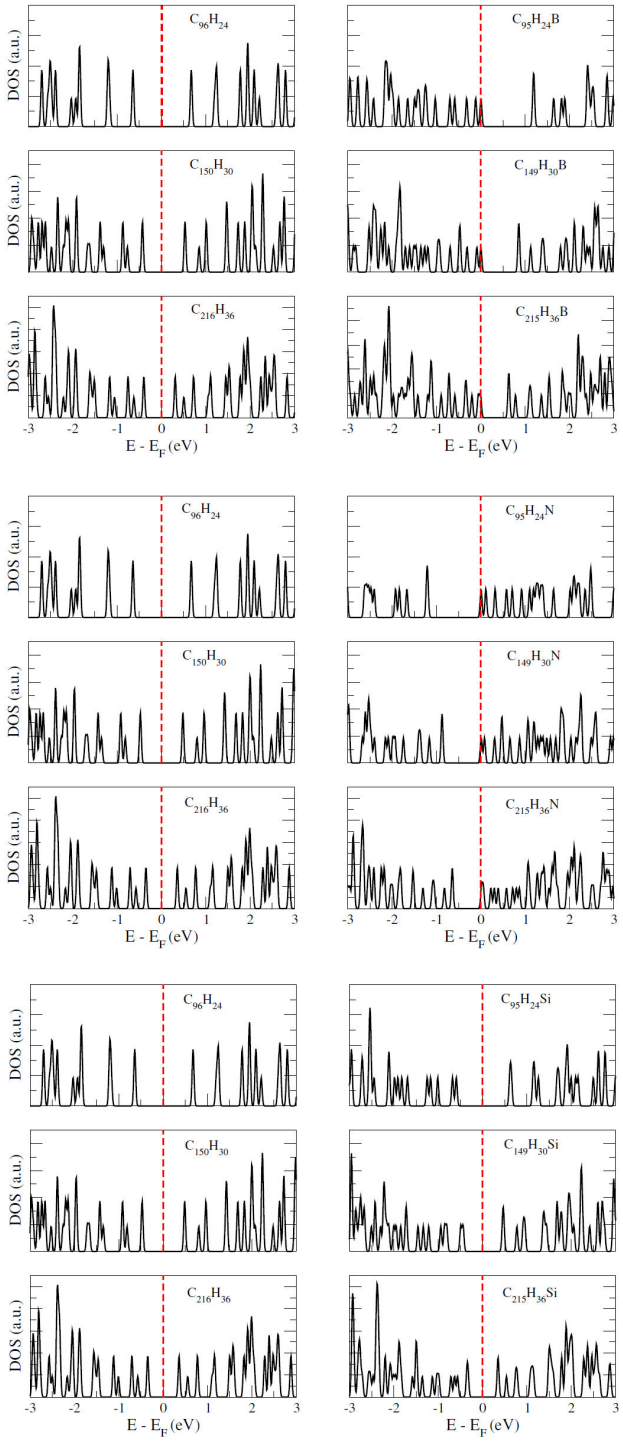

FIGURE 4. Density of states for C_mH_n (left column) and $C_{m-1}H_n\,S_a$ (right column), here S_a stands for substitutional atoms of boron (B), nitrogen (N), and silicon (Si). The (m, n) pair values are (96,24), (150,30), (216,36).

atom position, the carbon-to-silicon distance reaches 1.68 Å. For all the relaxed structures, as the substitutional atom has a larger atomic number, it increase the interatomic distance, slightly modifying the central hexagon. However, in all cases, the substitutional atom impurities are in the same plane as the carbon atoms.

The density of states results for the three largest hexagonal $C_{m-1}H_n\,S_a$ GQD, where S_a stands for the single substitutional (B, N, Si) atom, with (m,n) pairs of: (96,24), (150,30), and (216,36), are shown in Fig. 4. The DOS for the pristine C_mH_n GQD are in the left side for each case, and it is easy to see that the single substitutional impurities induce a richer DOS structure. For instance, in the firs set of plots from Fig. 4, which corresponds to the $C_{m-1}H_nB$ GQD, we can observe that, as the (m,n) pair increases, HOMO-LUMO molecule energy decreases, in a fashion similar to what is reported for the corresponding pristine case in the left side plot in each figure Most importantly, as the vertical red-dashed line represents the Fermi level (E_F), and it is crucial to notice that the boron substitutional atom acts as a p-type impurity, as expected. This is because the boron atom has only three valence electrons, leaving one acceptor energy level precisely at E_F. In the next three plot-set of Fig. 4, the n-type impurity nature of the nitrogen atom arises because its f ve valence electrons complete the carbon chemical bonds, leaving an unbound electron. Finally, for the single silicon substitutional atom, which has the same valence as the carbon atoms, it does not act as n- or p-type impurity, as can be clearly seen from the DOS results. However, it does induce local deformations as well as changes in the HOMO-LUMO in comparison with the pristine cases. The presence of a single doping impurity can induce n- or p-type nature to the GQD.

Figure 5 shows the ε_2 optical response for the $C_{m-1}H_n\,S_a$ system, considering boron, nitrogen and silicon substitutional atoms (S_a) with the same set of (m, n) pairs as those reported in Fig. 4. Here, we present the imaginary part of the dielectric function to observe the effect of the substitutional impurities on the system, considering polarized light in the x- and y-direction, as well as the effect of the GQD size. In the firs plot of Fig. 5 we present ε_2, with x-direction (black solid line) and y-direction (red dashed line) polarized light for the $C_{95}H_{24}B$ system. We can notice that, in comparison with the pristine case (see left column of Fig. 2),

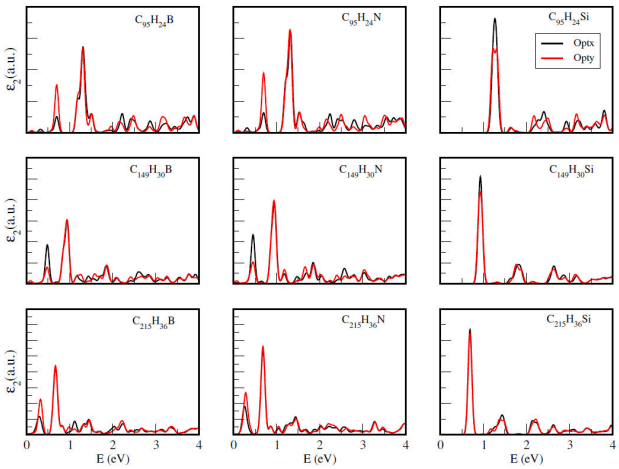

FIGURE 5. Imaginary part of the dielectric function, considering x- and y-direction polarized light, for $C_{m-1}H_n\,S_a$. Here, S_a stands for the substitutional atom (B, N,and Si).

it exhibits its firs maximum at approximately 1.25 eV, coinciding with the highest peak in the figure indicating that the optical response for energies less than 1 eV are completely attributed to the impurities. Also, the asymmetry in the hexagonal $C_{m-1}H_n\,S_a$ GQD, as can be seen from Fig. 3, induces small changes in ε_2 for polarized light in different directions, and we can easily observe that the y-directed optical response (red dashes line) is most intense that the x-directed one, at an energy about 0.75 eV. the same holds for the nitrogen atom case ($C_{95}H_{24}B$), but the ε_2 main peaks has higher values. Finally, in the last plot of the same line, that deals with the silicon doping impurity, we can see that there is no ε_2 optical response for energies less that the pristine main peak (about 1.25 eV) because, as the DOS results exhibits, this impurity does not act as an n- or a p-type impurity, just slightly diminishes the HOMO-LUMO energetic distance. In the same fashion, as the quantum dot size increase, the behaviour is analogous, but the ε_2 optical response experiences a redshift, in accordance with the DOS results in Fig. 4.

3.1.2. hexagonal GQD with two substitutional impurities

In this section, we discuss the effect of considering a second substitutional atom in the $C_{m-2}H_nS_{a_2}$ GQD. Here S_{a_2} represents two substitutional (B, N, Si) atoms, with one of them in the GQD's central hexagon and the second one at an arbitrary position, as well as in the *ortho*-, *meta*-, and *para*-position within the same central hexagon. For this study, we exclusively focus on the $C_{96}H_{24}$ GQD system because one (S_a) and two (S_{a_2}) substitutional atoms constitutes roughly 1% and 2% of the 96 carbon atoms in the structure, that can be considered a low impurity percentage.

Figure 6 shows the relaxed structure for the hexagonal $C_{94}H_{24}Si_2$ GQD and 7 its correspondingly HOMO-LUMO isosurfaces. In Fig. 6a), one Si atom is located in the central hexagonal ring, and the other one in positioned arbitrary, and there is no significan deviation from the hexagonal lattice shape. In Fig. 6b), we show the relaxed system with two Si atoms in *ortho*-director position, and significan local deformations can be observed. There appears to be an apparent overlap of the two Si atoms, which, of course, is not possible. However, the side view in the x-direction, shown in the bottom plot of the figure clarifie that the Si atoms depart from the plane with a Si-Si distance of 2.5 Å. This deviation can be explained because the Si atom is much larger ($z = 14$) than the C atoms ($z = 6$), and the electrostatic repulsion of their nuclei induces this effect. In Fig. 6c), we represent the *meta*-director position, which causes local deformations in the hexagon but maintains the atoms in the same plane as the C atoms. Figure 6d) shows the *para*-director position for silicon atoms, which also remains in the same plane than the C atoms but locally deforms the central hexagonal ring. The same applies to B and N substitutional atoms, although they are not depicted here. In both cases, even in the *ortho*-director position, the atoms remain in the same plane as the carbon ones, mainly because their corresponding atomic numbers

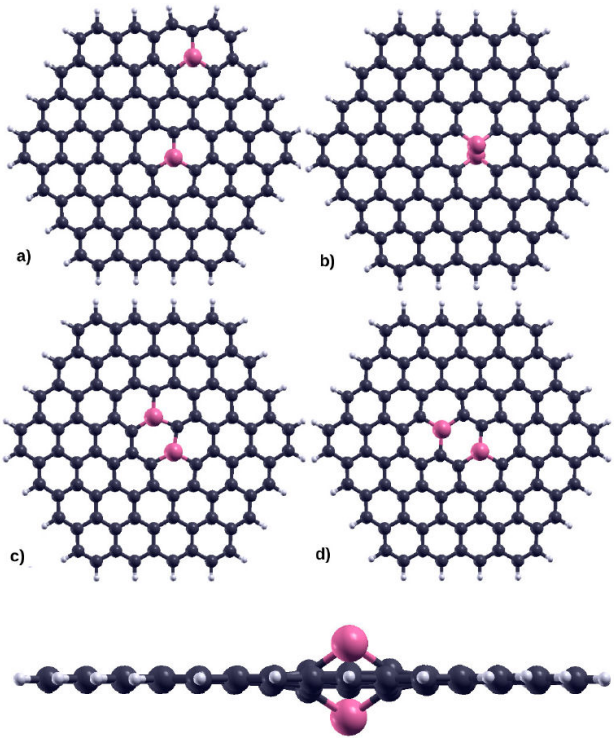

FIGURE 6. Relaxed structure for the hexagonal $C_{94}H_{24}Si_2$ GQD, with Si atoms located at: a) depicted random positions, b) *ortho*-, c) *meta*-, and d) *para*-directors. In the bottom plot, the side view for the *ortho*-director configuratio is shown.

are close to that of carbon. Therefore, depending on the location of the doping impurities an the electronic configuratio of the substitutional atom, as reflecte in the their respective atomic number, the local lattice distortion and optoelectronic properties will be affected.

Figure 7 represents the HOMO and LUMO isosurfaces for the case of double silicon substitutional atoms reported in Fig. 7. In all the reported configurations the HOMO and LUMO distributions are concentrated mainly on the silicon atoms. For the random position case, see Fig. 6a), we can observe that both HOMO and LUMO are distributed with triangular shape for the silicon atom near the center of the GQD but, not in this way for the one near the GQD boarder. The *ortho*-director configuratio is the most interesting one, at least for this substitutional atom, because as the silicon atoms leaves the x-y GQD plane, the HOMO and LUMO distributions are strongly located along the Si-Si line, as can be seen in the x-side view reported in the bottom plot of Fig. 7. The *meta*-director HOMO distribution exhibits more charge carrier density than the LUMO distribution, which is even more noticeable in the *para*-director configuration

To analyze the effect on the density of states of double boron, nitrogen and silicon substitutional atoms (S_{a_2}) located at random, *ortho*-, *meta*-, and *para*-director positions on the central hexagon of the $C_{m-2}H_nS_{a_2}$ GQD system, in Fig. 8, 9 and 10, we present the corresponding density of states for all the studied configurations The four plots in Fig. 8 correspond to the pristine and boron substitutional atoms

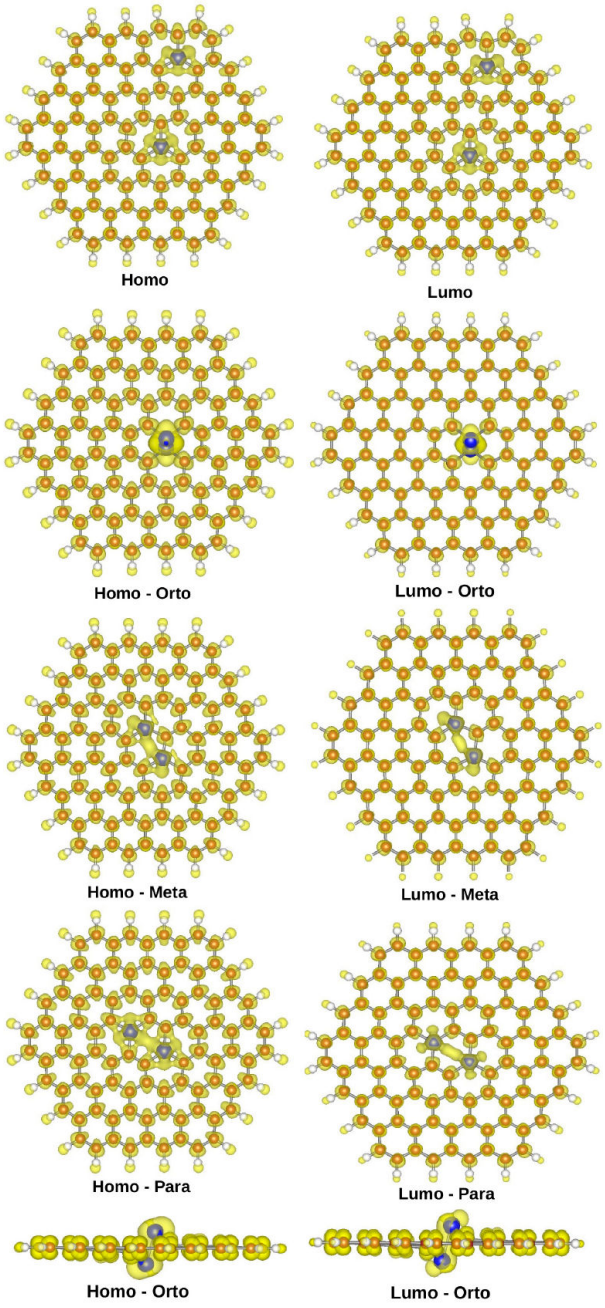

FIGURE 7. HOMO and LUMO isosurfaces representation for the hexagonal $C_{94}H_{24}Si_2$ GQD, with Si atoms located at: depicted random positions, *ortho*-, *meta*-, and *para*-directors, as reported in Fig. 6.

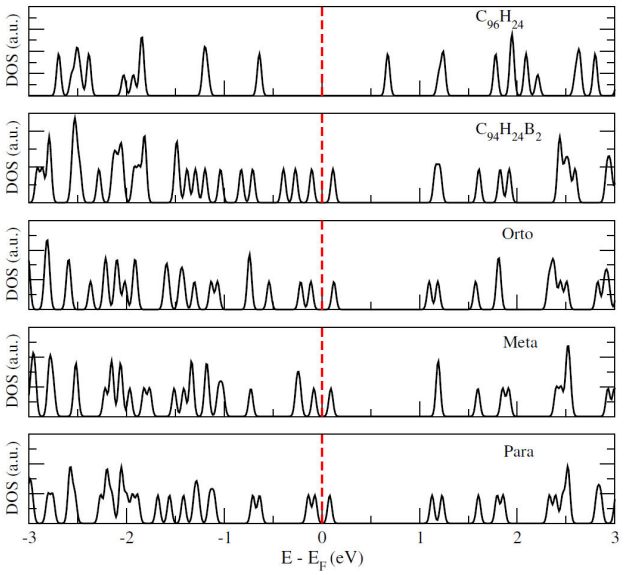

FIGURE 8. Density of states for the hexagonal $C_{96}H_{24}$ and $C_{94}H_{24}B_2$ doped GQD, with substitutional atoms at random, *ortho*-, *meta*-, and *para*-director positions.

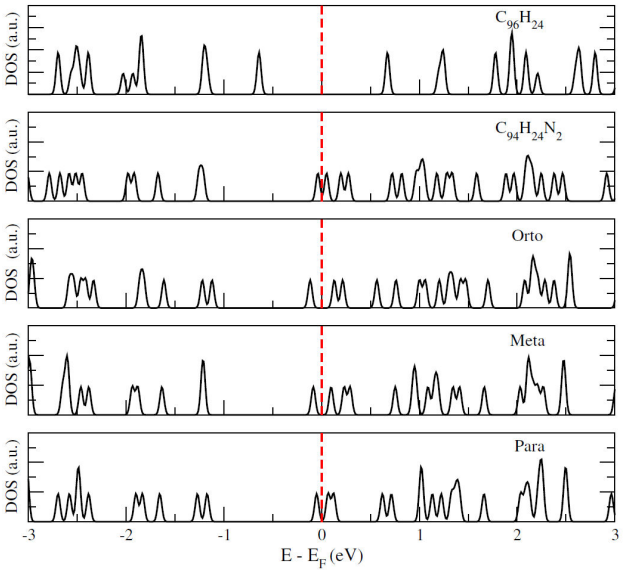

FIGURE 9. Density of states for the hexagonal $C_{96}H_{24}$ and $C_{94}H_{24}N_2$ doped GQD, with substitutional atoms at random, *ortho*-, *meta*-, and *para*-director positions.

of $C_{94}H_{24}B_2$ GQD, from top to bottom. Regardless of the positions of the two boron substitutional atoms, an unoccupied state very close to the highest occupied molecular orbital (HOMO) appears, indicating the p-type nature of the boron doping atom, which is located to the right of the Fermi level. Regarding the density of states (DOS) for the two different positions of boron substitutional atoms, we can observe that, in general, the DOS shape importantly depends on the boron atom's positions. For instance, for the random substitutional atom position configuration the lowest unoccupied molecular orbital (LUMO) -considering the hole state as an intermediate level-, has a Gaussian-like state shape at about 1.15 eV. For the *ortho*-director positions, the LUMO splits into two peaks, while for the *meta*-director positions, the peak position recedes further, increasing the HOMO-LUMO energy difference, and this has a sharp shape. Finally, for the *para*-director positions of boron substitutional atoms, it becomes splited once again.

In Fig. 9, corresponding to pristine and nitrogen substitutional atoms in the hexagonal $C_{94}H_{24}N_2$ GQD, they clearly act as n-type doping impurities because we can see an occupied state located to the left of the Fermi level energy, very

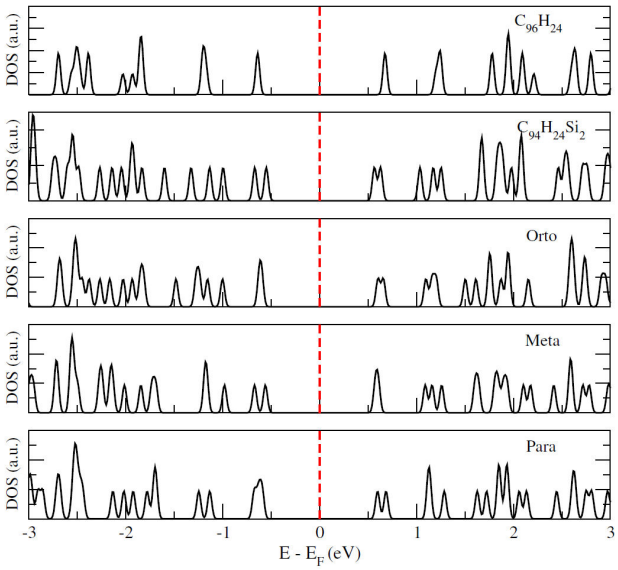

FIGURE 10. Density of states for the hexagonal $C_{96}H_{24}$ and $C_{94}H_{24}Si_2$ doped GQD, with substitutional atoms at random, *ortho*-, *meta*-, and *para*-director positions.

close to the LUMO state, with the lowest HOMO-LUMO energetic distance reported for the *ortho*-director configuration Finally, in Fig. 10, we present the DOS for the $C_{94}H_{24}Si_2$ GQD for all the chosen substitutional atoms positions, as well as the pristine case for comparison, and as expected because the substitutional atoms belongs to the same IVA group, there are no n- or p-type energy level. However, the density of states shape is clearly affected by the Si atoms, which will eventually influenc the optical properties, as we will discus in the following paragraph.

Figure 11 shows the imaginary part of the dielectric function (ε_2) for $C_{94}H_{24}S_{a_2}$ GQD, taking into account two (B, N, and Si) substitutional atoms at random, *ortho*-, *meta*-, and *para*-director positions. In the firs line of the Fig. 11, we report the $C_{94}H_{24}S_{a_2}$ GQD with B, N, and Si. We can observe a similar behavior as in the case of a single substitutional atoms, as reported in Fig. 5, but here ε_2 exhibits more structure for energies less than 1.0 eV in the case of boron and nitrogen substitutional atoms. When we compare double and single Si substitutional atoms, we can see a lower main peak with two Si atoms than with only one, at least for the chosen random position configuration We must stress here that the x- (black solid line) and y-direction (red solid line) polarized incident light dielectric function dependency does not reflec noticeable peak shifts but rather small differences in intensities.

Most importantly, the analysis of the double substitutional atoms at *ortho*-, *meta*-, and *para*-director positions is crucial, as reported in columns for each S_{a_2} case in Fig. 11, considering x- (black solid line) and y-directed (red solid line) polarized incident light. For instance, in the firs column of Fig. 11, we present the imaginary part of the dielectric function for the $C_{94}H_{24}B_2$ GQD. We can observe that for the *ortho*-director position ε_2 exhibits two peaks for energies

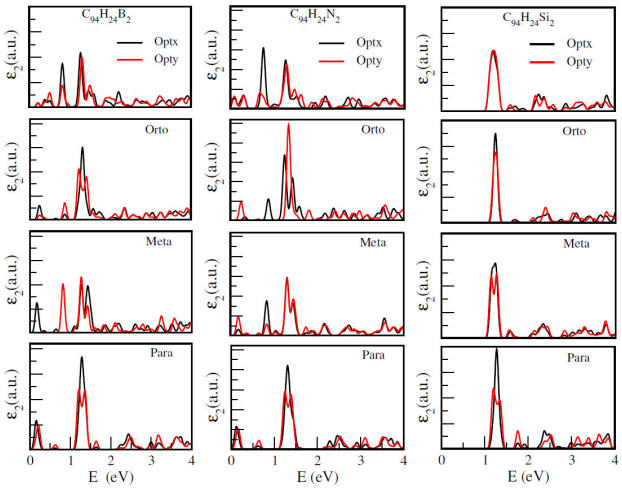

FIGURE 11. Imaginary part of the dielectric function (ε_2), with light polarization in x- and y-directions, with B, N, and Si substitutional atoms at random, *ortho*-, *meta*-, and *para*-director positions.

less than 1 eV, which are entirely due to the doping effect. The firs peak is most intense for x-direction polarized incident light, while for the second one, the y-direction polarized incident light predominates, we can also mention that the main peak splits for the case of y-directed polarized incident light only. When we focus on the *meta*-director configura tion, the two peaks due to the doping effect are still present, but they are more intense than in the previous case, especially the one corresponding to the y-direction polarized incident light. In comparison with the previous case, both peaks experience a redshift, and the main peak becomes split for both incident light polarizations. Finally, within the same column, we report the *para*-director' positions for the double boron substitutional atoms. Is is easily to observe that the ε_2 peaks, with x- and y-directed polarized incident light, recede further from the original main peak, which occurs at approximately 1.25 eV. Furthermore, the main peak splits only when the incident light is polarized in the y-direction, as happens for the *orto*-director configuration In the case of $C_{94}H_{24}N_2$ GQD, we observe a similar ε_2 behaviour for the *ortho*-director positions, but the x- and y-direction peaks behaviours are interchanged. For the *meta*-director configuration the main peak split is completely analog for both incident light polarizations, but the peaks due to the substitutional atoms are also interchanged. Finally, in the case of Si substitutional atoms, $C_{94}H_{24}Si_2$ GQD, the imaginary part of the dielectric function, with x- and y-directed polarized incident light, exhibits changes in width and height depending on the substitutional atom's position as well as on the incident light polarization, but without any optical response due to n- or p-type doping, as seen for boron and nitrogen.

4. Conclusions

In this paper, we reported the density of states for a hexagonal graphene quantum dot, as we increased the system size

for the pristine case, as well as the effect of single and double substitutional atoms of boron, nitrogen and silicon. We can conclude that as the GQD increases, the HOMO-LUMO energetic distance decreases. The boron atom acts as n-type doping impurity, and the nitrogen atom acts as a p-type one, for both single and double substitutional atom configurations The silicon atom slightly affect the DOS structure, but what is most important is the fact that only the *orto*-director positions push the silicon atoms out of the plane, that can be useful for eventually docking other molecules onto the system. From the imaginary part of the dielectric function results, in the case of single substitutional boron, nitrogen and silicon atoms, we found that as the system size increase it gives a small but noticeable effect on the peak intensities for x- and y-directed polarized incident light, specially for the boron and nitrogen substitutional atoms' imaginary part of the dielectric function peaks. When double-doping atoms are considered for the analysis of the imaginary part of the dielectric function, we reported a well differentiated ε_2 function shape, with clear anisotropy for x- and y-directed polarized incident light. We propose that this can be used to clearly determinate the type of substitutional atoms and their positions from optical measurements.

Acknowledgements

K. M. Méndez-Martínez acknowledge to CONAHCyT for the scholarship grant 935331. J. C. Martínez-Orozco acknowledge to CONACyT-SEP México for the partially finan cial support through the project number A1-S-8842.

1. K. S. Novoselov, Nobel Lecture: Graphene: Materials in the Flatland, *Rev. Mod. Phys*. **83** (2011) 837, https://doi.org/10.1103/RevModPhys.83.837.
2. H. S. ahin *et al*., Monolayer honeycomb structures of group-IV elements and III-V binary compounds: Firstprinciples calculations, *Phys. Rev. B* **80** (2009) 155453, https://doi.org/10.1103/PhysRevB.80.155453.
3. T. Gorkan, E. Aktürk, and S. Ciraci, Deformed octagonhexagon- square structure of group-IV and group-V elements and III-V compounds, *Phys. Rev. B* **100** (2019) 125306, https://doi.org/10.1103/PhysRevB.100.125306.
4. S. Manzeli, D. Ovchinnikov, D. Pasquier, O. Yazyev and A. Kis, 2D transition metal dichalcogenides, *Nat. Rev. Mater*. **5** (2017) 17033, https://doi.org/10.1038/natrevmats.2017.33.
5. K. James Singh *et al*., Recent Advances in Two-Dimensional Quantum Dots and Their Applications, *Nanomaterials* **11** (2021) 1549, https://doi.org/10.3390/nano11061549.
6. H. Abdelsalam and Q. F. Zhang, Properties and applications of quantum dots derived from twodimensional materials, *Adv. Phys.: X* **7** (2022) 2048966, https://doi.org/10.1080/23746149.2022.2048966.
7. J. Peng *et al.*, Graphene Quantum Dots Derived from Carbon Fibers, Nano Letters **12** (2012) 844, https://doi.org/10.1021/nl2038979.
8. S. Kundu *et al*., Synthesis of N, F and S co-doped graphene quantum dots, *Nanoscale* **7** (2015) 11515, https://doi.org/10.1039/C5NR02427G.
9. X. Wang *et al.*, Quantum dots derived from two-dimensional materials and their applications for catalysis and energy, *Chem. Soc. Rev*. **45** (2016) 2239, https://doi.org/10.1039/C5CS00811E.
10. A. Tiutiunnyk *et al.*, Electronic and magnetic properties of stacked graphene quantum dots, *Diam. Relat. Mater.* **131** (2023) 109550, https://doi.org/10.1016/j.diamond.2022.109550.
11. A. Tiutiunnyk *et al*., Electronic, Optical, and Magnetic Properties of Doped Triangular MoS2 Quantum Dots: A Density Functional Theory Approach, *phys. status solidi B* **259** (2022) 2100509, https://doi.org/10.1002/pssb.202100509.
12. B.-R.Wu, A DFT study for silicene quantum dots embedded in silicane: controllable magnetism and tuneable band gap by hydrogen, *RSC Adv.* **9** (2019) 32782, https://doi.org/10.1039/C9RA04705K.
13. J. J. HernÂ´andez Rosas *et al.*, First principles calculations of the electronic and chemical properties of graphene, graphane, and graphene oxide, *J. Mol. Model.* **17** (2011) 1133, https://doi.org/10.1007/s00894-010-0818-1.
14. S. J. Goettl *et al*., Gas-Phase Synthesis of Coronene through Stepwise Directed Ring Annulation, *J. Am. Chem. Soc*. **145** (2023) 15443, https://doi.org/10.1021/jacs.3c03816.
15. K. Harismah, M. Mirzaei, and R. Moradi, DFT Studies of Single Lithium Adsorption on Coronene, *Z. Naturforsch.* **73** (2018) 685, https://doi.org/10.1515/zna-2017-0458.
16. S. Sanyal, A. K. Manna, and S. K. Pati, Effect of Imide Functionalization on the Electronic, Optical, and Charge Transport Properties of Coronene: A Theoretical Study, *J. Phys. Chem. C* **117** (2013) 825, https://doi.org/10.1021/jp310362c.
17. J. Lüder, M. H. Cheow, and S. Manzhos, Understanding doping strategies in the design of organic electrode materials for Li and Na ion batteries: an electronic structure perspective, *Phys. Chem. Chem. Phys*. **19** (2017) 13195, https://doi.org/10.1039/C7CP01554B.
18. G. W. Ejuh *et al*., Electronic structure, physico-chemical, linear and non linear optical properties analysis of coronene, 6B-, 6N-, 3B3N- substituted C24H12 using RHF, B3LYP and wB97XD methods, *Opt. Quantum Electron.* **49** (2017) 382, https://doi.org/10.1007/s11082-017-1221-2.

19. F. Montejo-Alvaro *et al.*, DFT study of small gas molecules adsorbed on undoped and N-, Si-, B-, and Al-doped graphene quantum dots, *Theor. Chem. Acc.* **138** (2019) 37, https://doi.org/10.1007/s00214-019-2428-z.

20. P. Zhang *et al.*, Size effect of oxygen reduction reaction on nitrogen-doped graphene quantum dots, *RSC Adv.* **8** (2018) 531, https://doi.org/10.1039/C7RA10104J.

21. Q. Guo *et al*., Effects of hydronium and hydroxide ion/group on oxygen reduction reaction electrocatalytic activities of Ndoped graphene quantum dots, *Mol. Catal*. **517** (2022) 112009, https://doi.org/10.1016/j.mcat.2021.112009.

22. H.-C. Li *et al*., How does the porphyrin-like vacancy affect the spectral properties of graphene quantum dots? A theoretical study, *J. Phys.-Condens. Mat*. **32** (2020) 155902, https://doi.org/10.1088/1361-648x/ab62bb.

23. M. A. Abdelati *et al.*, Pristine and holey graphene quantum dots: Optical properties using time independent and dependent density functional theory, *Physica E* **128** (2021) 114602, https://doi.org/10.1016/j.physe.2020.114602.

24. J. Feng *et al*., Density functional theory study on optical and electronic properties of co-doped graphene quantum dots based on different nitrogen doping patterns, *Diam. Relat. Mater.* **113** (2021) 108264, https://doi.org/10.1016/j.diamond.2021.108264.

25. D. Mombrú *et al.*, Curvature and vacancies in graphene quantum dots, *Appl. Surf. Sci*. **462** (2018) 540, https://doi.org/10.1016/j.apsusc.2018.08.141.

26. J. M. Soler *et al.*, The SIESTA method for ab initio order-N materials simulation, *J. Phys.-Condens. Mat.* **14** (2002) 2745, https://doi.org/10.1088/0953-8984/14/11/302.

27. A. García *et al*., Siesta: Recent developments and applications, *J. Chem. Phys.* **152** (2020) 204108, https://doi.org/10.1063/5.0005077.

28. F. Flores, J. Ortega, and H. Vázquez, Modelling energy level alignment at organic interfaces and density functional theory, *Phys. Chem. Chem. Phys*. **11** (2009) 8658, https://doi.org/10.1039/B902492C.